Experimental and numerical comparison of multi-layered La(Fe,Si,Mn)13Hy active magnetic regenerators

Navickaité, Kristina; Bez, Henrique Neves ; Lei, Tian; Barcza, Alexander; Vieyra, Hugo ; Bahl, Christian; Engelbrecht, Kurt

Published in:
International Journal of Refrigeration

Link to article, DOI:
10.1016/j.ijrefrig.2017.10.032

Publication date:
2018

Document Version
Publisher's PDF, also known as Version of record

International Journal of Refrigeration 86 (2018) 322–330

Contents lists available at ScienceDirect

International Journal of Refrigeration

journal homepage: www.elsevier.com/locate/ijrefrig

Experimental and numerical comparison of multi-layered $La(Fe,Si,Mn)_{13}H_y$ active magnetic regenerators

Kristina Navickaitė[a,*], Henrique Neves Bez[b], Tian Lei[a], Alexander Barcza[c], Hugo Vieyra[c], Christian R.H. Bahl[a], Kurt Engelbrecht[a]

[a] Department of Energy Conversion and Storage, Technical University of Denmark, 4000 Roskilde, Denmark
[b] The Ames Laboratory of the US DOE, Iowa State University, Ames, IA 50011-3020, USA
[c] Vacuumschmelze GmbH & Co. KG, 63450 Hanau, Germany

ARTICLE INFO

Article history:
Received 29 June 2017
Revised 23 October 2017
Accepted 24 October 2017
Available online 7 November 2017

Keywords:
Magnetic cooling
First order materials
Magnetocaloric effect
Regeneration
Modelling

ABSTRACT

We present an experimental and numerical comparison of epoxy bonded multi-layered $La(Fe,Si,Mn)_{13}H_y$ active magnetic regenerators. First, no-load tests were performed on four regenerators with two layers of material and varying amounts of epoxy (from 1 wt% to 4 wt%) in order to find the amount of epoxy necessary to maintain the mechanical integrity of the regenerators. As the second part of the study, experimental results of two regenerators with five and nine layers are compared to predictions from the one-dimensional numerical model. A maximum temperature span, ΔT_{span}, over 20 K was measured and it is effectively equal for both regenerators. The numerical modelling was generally in good agreement with experimental results.

1. Introduction

Magnetic refrigeration (MR) is a promising alternative to conventional vapour compression technology, and an active research topic for magnetocaloric materials and system performance. It is an appealing technology since the theoretical energy efficiency of a well-designed system is equal or even larger than that of conventional refrigeration (Gschneidner and Pecharsky, 2008). Moreover, MR uses no greenhouse or ozone-depleting gases (Jacobs et al., 2014), as solid magnetocaloric materials (MCM) are used as the refrigerant. MCMs exhibit changes in temperature and entropy upon a change in external magnetic field.

According to the phase transition, MCMs can either undergo a first order phase transition (FOPT) or a second order phase transition (SOPT). A SOPT between the non-magnetic and magnetic phase results in a continuous entropy change across a broad temperature range. A first order phase transition (FOPT) results in a very narrow and sharp entropy change as a function of temperature. Although most FOPT materials exhibit a large magnetocaloric effect, other challenges to implementing them in a high performance MR system accompany them. In addition to the magnetocaloric effect being large over only a narrow temperature range, they often exhibit thermal and magnetic hysteresis. Furthermore, FOPT materials are accompanied by a change either in the crystal volume or crystal structure, which can lead to cracking and mechanical instability (Bez Neves et al., 2016; Brück et al., 2004).

The $La(Fe,Mn,Si)_{13}H_y$ intermetallic material family has attracted significant attention as a FOPT material and is the subject of this study. The Curie temperature, T_C, of this compound can be tuned by substituting Fe with Mn. The T_C of an $La(Fe,Mn,Si)_{13}H_y$ material decreases monotonically with increased Mn concentration (Basso et al., 2015; Bratko et al., 2016). At a certain concentration of Mn, the phase transition becomes second order with no hysteresis. Thus, it was suggested that by using Mn it is possible to prepare weakly first order materials, which would provide high magnetocaloric properties without hysteresis even at a low magnetic field of about 0.5 T (Basso et al., 2015).

$La(Fe,Mn,Si)_{13}H_y$ exhibits changes in volume during the phase transition, causing brittleness when the material is cycled magnetically. Thus, porosity was introduced as a tool to avoid cracking of the material over the (de)magnetization cycles, as suggested by Lyubina et al. (2010). The porosity, which was obtained by crushing and re-pressing dense bricks of the material, leads to the removal of grain boundaries. Subsequently the volume expansion that appears at the phase transition can take place more freely without damaging the material. However, induced porosity did not prevent

* Corresponding author.
E-mail address: knav@dtu.dk (K. Navickaitė).

https://doi.org/10.1016/j.ijrefrig.2017.10.032

Nomenclature

Abbreviations

AMR	active magnetic regenerator
COP	coefficient of performance
FOPT	first order phase transition
Fe	iron
Gd	gadolinium
HEX	hot heat exchanger
MCE	magnetocaloric effect
MCM	magnetocaloric material
Mn	manganese
MR	magnetic refrigeration
SOPT	second order phase transition
VSM	vibration sample magnetometer

Variables

a_c	cross section area
a	specific area
c	specific heat
d_h	hydraulic diameter
H	magnetic field
k	thermal conductivity
m	Mass
$\dot{m}$	mass flow rate
Nu	Nusselt number
P	pressure drop
S	specific entropy
ΔS	entropy change
T	temperature
T_C	Curie temperature
ΔT_{ad}	adiabatic temperature change
ΔT_{span}	temperature span
t	time
U	utilisation
V_h	total volume of the housing
v	Velocity
x	axial position

Greek letters

ε	porosity
ρ	density

Subscripts

e	epoxy
disp	dispersion
f	fluid
H	magnetic field
reg	regenerator
s	solid
stat	static

the material from disintegrating during extended operation in an active magnetic regenerator (AMR). A compound of MCM and thermoplastic (epoxy) was tested as a further possible solution in order to prevent regenerators from fragmenting and at the same time to shape the material (Lanzarini et al., 2015). Once the MCM and the epoxy are cured together, there is no chemical interaction between them. Thus, the epoxy itself does not change the magnetocaloric properties or T_C of the MCE.

One of the major challenges to deal with for FOPT materials is the narrow temperature range over which a significant MCE appears. Literature shows that it might be solved by constructing regenerators with successive layers each with a different T_C (Richard et al., 2004; Zimm et al., 2005). The T_C of each layer is chosen according to the temperature gradient desired in the regenerator. Modelling results show the effect of layering MCM with different T_C and how important the accuracy of the T_C distribution is along a regenerator (Lei et al., 2015). Here the authors showed that the optimal temperature span between two neighbouring layers is around 2.5 K for materials such as $La(Fe,Mn,Si)_{13}H_y$. This spacing produces 90% of the cooling power that would be obtained in an infinitely layered bed. It is also shown that an uneven distribution of T_C along the regenerator may lead to at least a 17% performance reduction when the standard deviation of T_C is 0.6 K. Moreover, Monfared and Palm (2015) emphasized the difference in T_C selection for each layer when a regenerator is designed either for maximum temperature span and/or seeking to maximise the Carnot efficiency.

Although the majority of AMR devices in the literature use SOPT materials (Kitanovski et al., 2015), some experimental studies using FOPT materials have been reported. Regenerators based on $La(Fe,Si)_{13}H_y$ or MnFePAs have been tested in both reciprocating and rotary devices (Bahl et al., 2017; Bez Neves et al., 2016; Govindappa et al., 2017; Jacobs et al., 2014; Lei et al., 2018). Notably a large-scale rotary device developed by Astronautics Corporation of America (Jacobs et al., 2014) used six layers of FOPT $La(Fe,Si)_{13}H_y$ spheres with T_C ranging from 303.6 to 316.2 K. With a total mass of the MCM 1.52 kg the device provided 2.5 kW cooling power at a temperature span of 11 K and coefficient of performance (COP) of 1.9. The operating frequency of the machine was 4 Hz.

In this paper, we present a comparison between experimental and numerical results of the performance of multi-layered $La(Fe,Si,Mn)_{13}H_y$ regenerators having two, five and nine layers. The model has been presented previously and verified against SOPT experimental results (Lei et al., 2017). AMR modelling is an active research topic and many models have been reported in the literature. Models using a 1D porous approach have been widely reported, including Plaznik et al. (2013), Vuarnoz and Kawanami (2013), Trevizoli et al. (2016), and Mugica Guerrero et al. (2017). 2D AMR models have been presented using a porous construction Liu and Yu (2010), by directly modelling a regenerator geometry that emulates spheres (Aprea et al., 2015) and by directly modelling flow between MCM plates (Tura et al., 2012). A detailed 3D model that directly models the regenerator geometry has also been reported by Bouchard et al. (2009). The vast majority of model results, especially those that are compared directly to experiments, have been generated for SOPT materials, and those are almost exclusively based on Gd and its alloys. Jacobs et al. (2014) presented good agreement between a 1D porous model and FOPT LaFeSiH materials. In this paper, the porous 1D model is used as a check of experimental results that the behaviour is as expected and there are no large discrepancies between expected results and experiments.

All investigated regenerators were made of epoxy bonded irregular particles. The total height of all the tested regenerators was the same, resulting in varying layer thicknesses. We also investigated the optimal amount of epoxy necessary to maintain the mechanical integrity of the regenerators. The results of no-load experiments showed that the temperature spans reported in this paper are the largest ever obtained in this small-scale test machine, emphasising the potential of $La(Fe,Mn,Si)_{13}H_y$ materials.

2. Experimental procedure

Vacuumschmelze GmbH provided six regenerators made of $La(Fe,Si,Mn)_{13}H_y$ irregularly shaped particles with a particle size between 250 µm and 500 µm. The particles were bonded into plastic housings having a height of 40 mm and an inner diameter of 30 mm and 34 mm for the two-layered beds and for five- and nine-layer beds, respectively, using epoxy (Fig. 1). Four of the tested regenerators were constructed in two layers (Fig. 2) and each of the

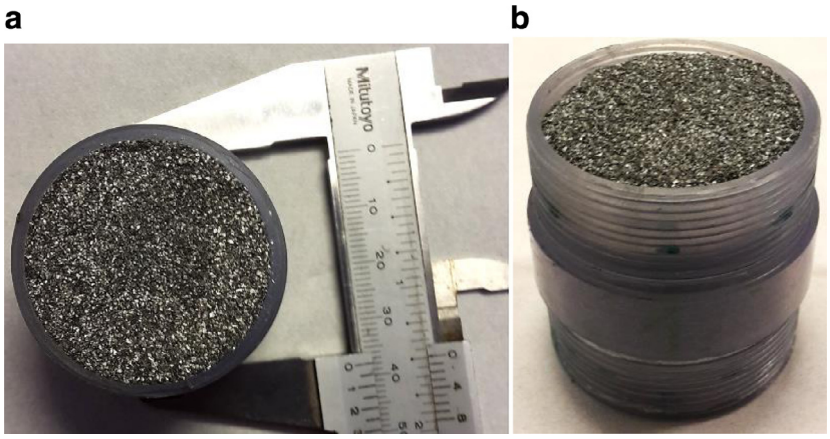

Fig. 1. The regenerators tested in the versatile machine: a) the sample with five layers of MCM before the tests (the housing is fully filled with the MCM until the top) and b) the sample with five layers of MCM after the no-load tests. The small gap on the top of the regenerator shows significant losses of MCM during the experiments.

Table 1
The properties of the tested regenerators.

	Inner dimensions, (diameter x height) (mm)	Overall mass of MCM (g)	Porosity (vol%)	Mass fraction of epoxy (wt%)
Regenerators with two layers	30 × 40	94.1	50	1
		93.1	48	2
		93.0	45	3
		91.2	43	4
Regenerators with five layers	34 × 40	122.9	47	2
Regenerators with nine layers		126.0	45	

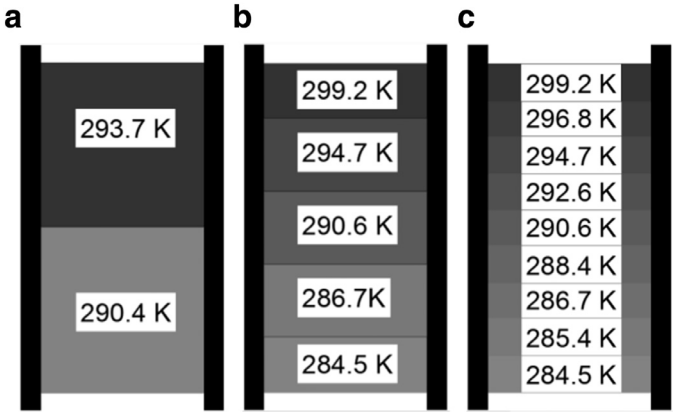

Fig. 2. Schematic drawings of a) two-layered, b) five-layered and c) nine-layered regenerator with T_c of each layer.

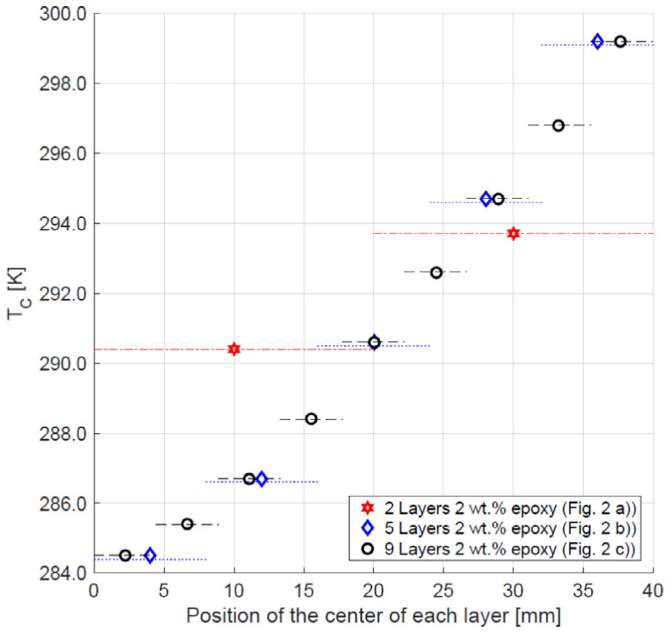

Fig. 3. T_C distribution over a regenerator bed. The colour guidelines represent layer thickness in each bed.

regenerators had a different amount of epoxy varying from 1 wt% to 4 wt%. Two other regenerators were fabricated after the experimental investigation to determine the necessary amount of epoxy was conducted. They were constructed with the same amount of epoxy as the best performing two-layer regenerator, but with more layers (Fig. 2). The T_C distribution along the regenerators is presented in Figs. 2 and 3. The T_C of each material was measured in a Lake Shore 7407 Vibrating Sample Magnetometer (VSM) using a sample mass of each material of approximately 10 mg. The applied field for the measurements was 10 mT and the Curie temperature was defined as an inflection point of the magnetisation in that field. The Curie temperature defined in this way will be lower than the temperature at which ΔS or ΔT_{ad} have their maximum (Smith et al., 2012).

The regenerators are described in more detail elsewhere (Bez Neves et al., 2016). The porosity ε was estimated for each regenerator using Eq. (1) and is shown in Table 1.

$$\varepsilon = 1 - \frac{\frac{m_s}{\rho_s} + \frac{m_e}{\rho_e}}{V_h} \quad (1)$$

where V_h is the total inner volume of the housing, m_s and m_e are the masses of the solid and epoxy, respectively, and ρ_s and ρ_e are the densities of the solid and epoxy, respectively. The values for ρ_s and ρ_e are 7000 kg m^{-3} and 1250 kg m^{-3}, respectively.

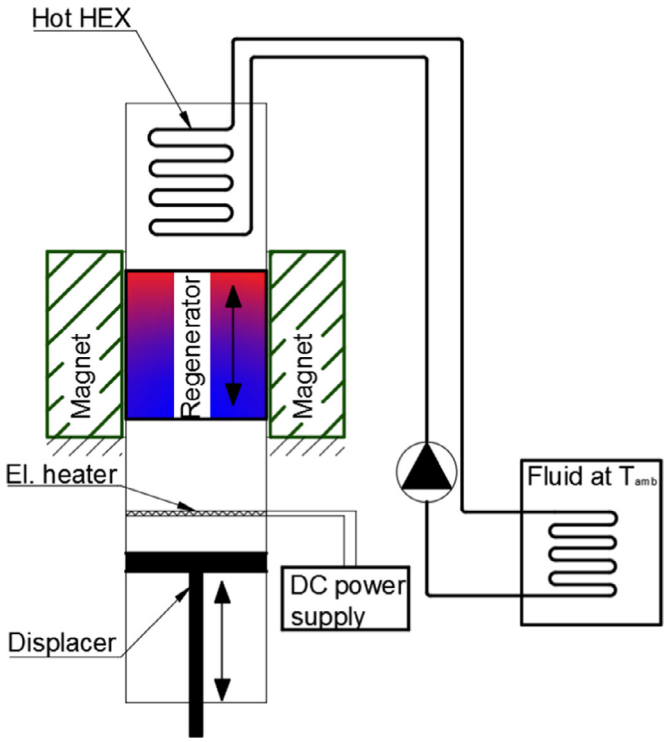

Fig. 4. The schematic drawing of the testing device.

The regenerators were tested in a versatile small-scale reciprocating device described previously in Bahl et al. (2008). Fig. 4 shows the schematic drawing of the test machine, which is placed inside a commercial refrigerator with a temperature-control system. The test machine consists of a Halbach array permanent magnet that is placed at a fixed position. The average generated magnetic field inside the magnet bore (ø 40 mm) is 1.1 T. A regenerator is moved in and out of the magnetic field by a stepper motor, and a displacer, placed at the cold side of the regenerator, provides reciprocating flow of the heat transfer fluid timed to the changes in magnetic field. The design of the device enables testing of a relatively small amount of MCM for varying operational parameters, such as the cycle frequency, utilisation and hot side temperature. A wire heater (Fig. 4) is used as a heating load at the cold side of the regenerator. The applied heating power is controlled via an Aim TTi EL302P power supply varying voltage and registering current. The stated power accuracy is ± 0.9%. Temperatures are measured by calibrated E-type thermocouples placed at the hot and cold sides of the test setup and inside the temperature controlling cabinet. The measurement error is ± 0.5 K.

The temperature at the hot side of the setup is maintained by a forced convection heat exchanger, which is placed in the cabinet. Note that the heat transfer fluid, which is in thermal connection with the solid, is hydraulically independent from the fluid circulating in the heat exchanger loop. Thus, we control the hot end temperature when controlling ambient temperature. The flow characteristics such as velocity and flow rate are changed by modifying the speed and the amplitude of the displacer movement, respectively. One of the most important parameters for testing regenerators is utilisation. It is a dimensionless parameter describing the ratio between the thermal mass of the fluid pushed through the regenerator per one cycle and the thermal mass of the solid. The utilisation U is defined here as:

$$U = \frac{m_f c_f}{m_{reg} c_s} \tag{2}$$

where m_f is the mass of the fluid pushed through the regenerator in one direction, c_f the specific heat of the fluid, m_{reg} the mass of the regenerator and c_s is the specific heat of the regenerator material (Kitanovski et al., 2015). The values used for c_f and c_s are 4210 J kg^{-1} K^{-1} and 501 J kg^{-1} K^{-1} (Basso et al., 2015), respectively. Note that the utilisation is defined using the background value of c_s rather than the peak value.

3. Numerical modelling

Numerical modelling is a powerful tool to study the AMR performance. In this paper, a 1D numerical model is used to investigate and predict the theoretical performance of the presented regenerators. The model was developed and presented elsewhere (Lei et al., 2015), and has previously been validated against SOPT materials. However, it has not been verified against multi-material FOPT materials and here it is used to check that model predictions are in general agreement with experimental results. The modelling is used to verify that the regenerators are constructed properly and that the MCM is behaving as expected. The model is based on two energy equations for the solid refrigerant and fluid (Lei et al., 2015), as shown in Eqs. (3) and (4). It is assumed that the fluid is incompressible and the regenerator housing is adiabatic.

$$\frac{\partial}{\partial x}\left(k_{stat} A_c \frac{\partial T_s}{\partial x}\right) + \frac{Nuk_f}{d_h} a_s A_c (T_f - T_s) = A_c (1-\varepsilon)\rho_s \left[c_H \frac{\partial T_s}{\partial t} + T_s \left(\frac{\partial s_s}{\partial H}\right)_{T_s} \frac{\partial H}{\partial t}\right] \tag{3}$$

$$\frac{\partial}{\partial x}\left(k_{disp} A_c \frac{\partial T_f}{\partial x}\right) - \dot{m}_f c_f \frac{\partial T_f}{\partial x} - \frac{Nuk_f}{d_h} a_s A_c (T_f - T_s) + \left|\frac{\partial P}{\partial x}\frac{\dot{m}_f}{\rho_f}\right| = A_c \varepsilon \rho_f c_f \frac{\partial T_f}{\partial t} \tag{4}$$

where: k, T, ρ, c, and s are the thermal conductivity, temperature, density, specific heat, and specific entropy; A_c, d_h, a_s, and ε are the cross section area, hydraulic diameter, specific area, and porosity, which reflect the geometry characteristics of a regenerator; x, t, $\dot{m}$, and H are the axial position, time, mass flow rate, and internal magnetic field. The subscripts f and s represents fluid and solid refrigerant, respectively, $\frac{\partial P}{\partial x}$ is pressure drop, and Nu is Nusselt number.

The two terms on the left hand side of Eq. (3) represent the thermal conduction through the regenerator bed and the heat transfer between the fluid and MCM. The term on the right hand side determines the energy storage and magnetic work of the solid. From the left hand side the thermal conduction (the first term), enthalpy flow (the second term), heat transfer with the solid (the third term), viscous dissipation (the fourth term) and energy storage for the fluid (the right hand side) are described by Eq. (4). Nielsen and Engelbrecht (2012) gives explicit explanation for the static thermal conductivity and due to the fluid dispersion, Nusselt number and pressure drop. One can note that both equations are coupled by the heat transfer term, and they are solved numerically by discretising in time and spatial domains. More details about the model and related expressions of each term are given in Lei et al. (2016).

It should be noted that the effect of epoxy was not included in the model. This is because the mass of epoxy is small in comparison to the mass of fluid and solid. In the results section below, it is shown that there is a noticeable effect due to the presence of epoxy, but the difference is similar to the expected level of uncertainty in the modelling due to uncertainties in the geometry and material properties.

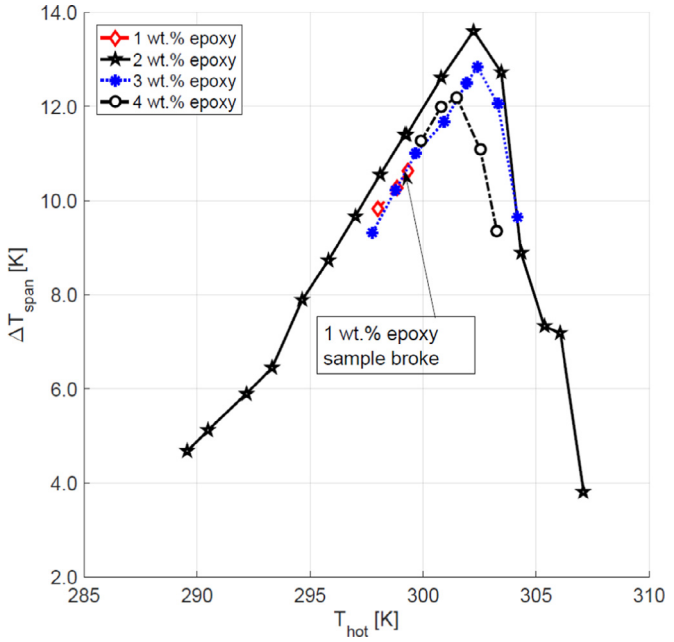

Fig. 5. The steady state temperature span between the hot and the cold side as a function of hot side temperature at different epoxy ratios in the tested two-layer regenerators.

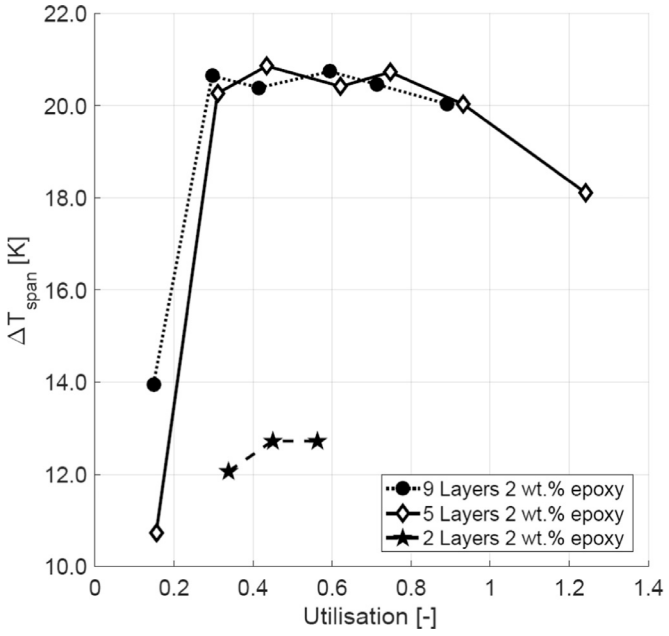

Fig. 6. The steady state temperature span between the hot and the cold side as a function of the utilisation at no-load at hot side temperature 30 °C and best-case flow velocity.

4. Results and discussion

A water-based solution with 2 wt% of the corrosion inhibitor Entek FNE was used as the heat transfer fluid. Even though the MCM is epoxy bonded into regenerators, it is susceptible to corrosion in aquatic systems because parts of the MCM are directly exposed to the fluid. Firstly, the best operational point for the regenerators was determined by a series of experiments at constant hot end temperature. The optimal fluid velocity, v_f, was found while holding the utilisation constant. The optimal utilisation was found while holding the fluid velocity constant at the optimum and varying the fluid displacement. Note that the cycling speed changed when the utilisation or fluid velocity was changed. The optimal operational point at which the performance of the two-layer regenerators at no-load experiments were tested was $U = 0.45$ and $v_f = 8.2$ mm s^{-1}. The cycling speed at the operational point was approximately 0.15 Hz.

The two-layer regenerators were tested to determine the effects of varying epoxy amounts. Fig. 5 gives the no-load temperature span across each regenerator for a range of hot side temperatures. One can see that the maximum temperature spans are $\Delta T_{span} = 13.6$ K, 12.8 K and 12.2 K for the samples with 2 wt%, 3 wt% and 4 wt% of epoxy, respectively. The regenerator with 1 wt% epoxy could not withstand the forces during the test and disintegrated before adequate results could be obtained. Thus, the test could not be finished.

The first series of experiments showed that the epoxy itself does affect the performance of the regenerators negatively when the amount is increased. This is because the epoxy is a passive material, which is also a poor thermal conductor. The larger mass fraction of epoxy leads to a reduction in both the mass fraction of active material and the heat transfer in the bed. Summarising the first series of experiments, it is concluded that 2 wt% of epoxy is the optimum for the two-layer regenerators. Based on these results, two more regenerators with more layers were constructed with 2 wt% epoxy (Figs. 1 and 2).

The two, five and nine-layer regenerators with 2 wt% epoxy were then tested at no-load conditions varying the utilisation. The optimal operational flow velocity v_f for five and nine-layer beds were 21.7 mm s^{-1} and 22.7 mm s^{-1}, respectively. The no-load temperature span of each bed at the reported optimal flow velocity as a function of utilisation is shown in Fig. 6. One can see that even at similar utilisations of 0.45, 0.43 and 0.42 for two, five and nine layer regenerators, respectively, the temperature is more than 8 K higher for the five- and nine-layer regenerators than for the two-layer regenerator. It is noticeable from Fig. 6 that utilisation does not have a strong influence on the no-load performance of regenerators with five and nine layers in a range from 0.3 to 0.9, but at relatively low or high values of the utilisation performance decreases drastically. This weak dependence of the temperature span on utilisation was also reported by Bez Neves et al. (2016) for similar regenerators with one and two layers. In comparison, a Gd-based single layer AMR showed stronger dependency of performance on utilisation (Engelbrecht et al., 2013; Tušek et al., 2014).

Later, the regenerators were characterised varying the hot side temperature. As it is shown in Fig. 7, the maximum temperature span established by a two-layer regenerator is much lower than the maximum temperature of five and nine-layer regenerators. This is a consequence of the five- and nine-layer regenerators having a larger range of Curie temperatures than the regenerator with two layers (Fig. 2).

One could note that the utilisation of the five-layer regenerator is approximately two times bigger than of two- and nine-layer regenerators. This is due to initially chosen operational temperature point. Firstly the five- and nine-layer regenerator were tested at 305.5 K hot side temperature to define the optimal utilisation. Obtained results (not presented in this paper) showed that the optimal utilisations for five- and nine-layer regenerators are 0.93 and 0.42, respectively. Further experiments showed that the optimal working temperature for both regenerators is approximately 303 K. Therefore, we can conclude the more layers a regenerator has the more sensible it is to any changes in operational point, especially hot side temperature changes.

Numerical studies predict that the more layers a regenerator has, the better the performance is and a higher specific cooling power is obtained, although there is a diminishing gain in

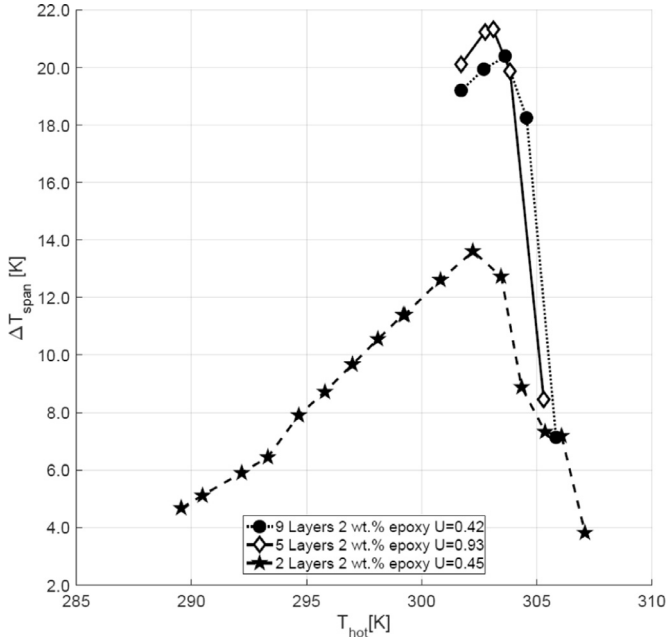

Fig. 7. The steady state no-load temperature span between the hot and the cold side as a function of hot side temperature for two-, five- and nine-layer regenerators.

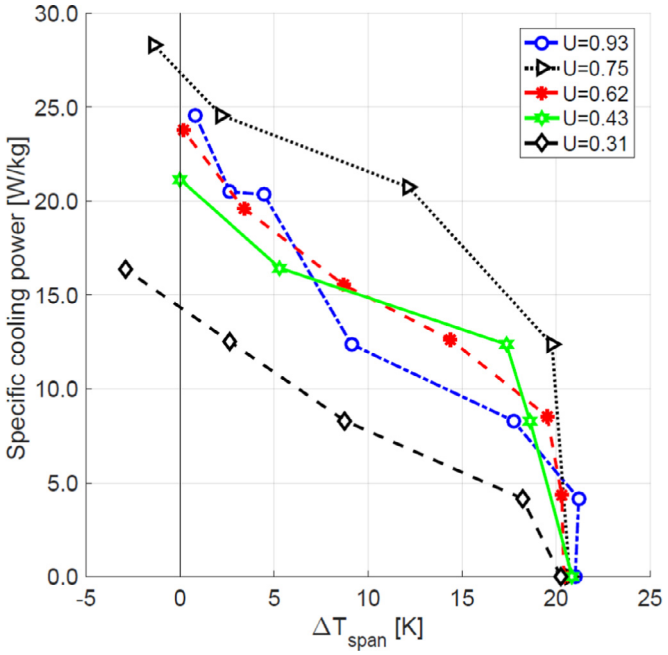

Fig. 8. The cooling power of the material with five layers as a function of temperature span obtained at several different utilisations at the constant hot side temperature of 303 K. The maximum applied cooling power for this regenerator was 3.5 W.

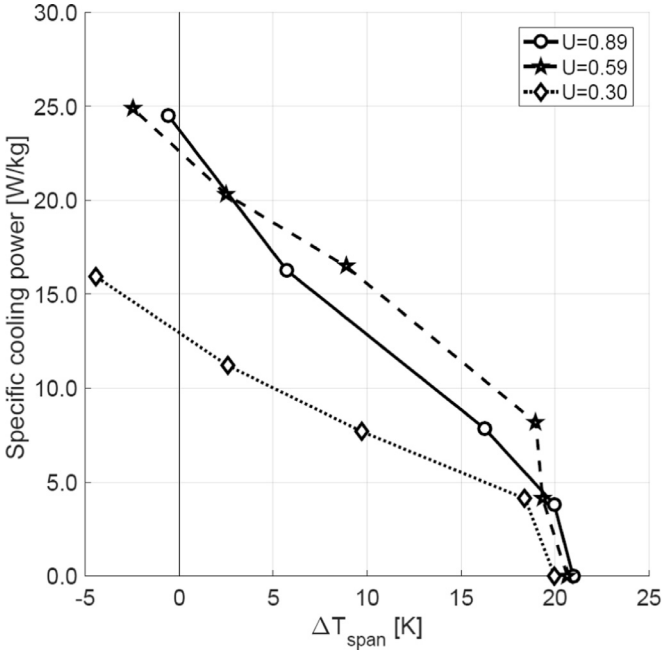

Fig. 9. The cooling power of the material with nine layers as a function of temperature span obtained at several different utilisations at the constant hot side temperature of 303 K. The maximum applied cooling power for this regenerator was 3.5 W.

performance as the number of layers increases above a certain level (Lei et al., 2015). The same study concludes that in order to get 90% of cooling power at maximum field of 1.2 T the temperature gap between two neighbouring layers should be around 2.5 K. It is noticeable that FOPT materials require 4–6 times more layers than SOPT to achieve the maximum temperature span (Lei et al., 2016). From Fig. 3 it is evident that the distribution in T_C of the tested regenerators is close to but not completely even. This may be the reason that the nine-layer regenerator did not perform better than the five-layer one. Another possible explanation is that the layer thickness of the nine-layer regenerator was too small. Therefore, it cannot successfully establish larger temperature span than the five-layer regenerator (Govindappa et al., 2017).

Cooling load tests were performed at different utilisations for both the five-layer and nine-layer regenerators (see Figs. 8 and 9). Both regenerators showed similar results and established a temperature span up to $\Delta T = 18$ K under a specific heat load of 5 W kg^{-1}. Note that the blown fluid mass through both regenerators was the same for all the corresponding experiments. The slight difference in utilisation and the applied specific power is due to a slight difference in the regenerator mass, used for calculations. Jacobs (2009, 2013) and Tušek et al. (2014) reported that the cooling power drops drastically as soon as the span exceeds the range of Curie temperatures in the bed, as is also observed in Figs. 8 and 9. Teyber et al. (2016) showed that cooling power of SOPT material two-layer regenerators highly depends on the transitional temperature between layers. We found that the highest cooling capacity is achieved at utilisations of around 0.75. This effect is a combination of magnetocaloric and heat transfer properties of the beds. Therefore, at this utilisation point, enough fluid was pushed through to maintain a high cooling power and it was small enough not to destroy the temperature span. In other words, the operational temperature of each layer was close enough to its transitional temperature.

The temperature of the thermal reservoir at HEX was set to be constant for all the experiments. However, the measured value of the hot side temperature increased from 303.5 K to 304.4 K for the five-layer regenerator and from 303.3 K to 303.9 K for the nine-layer regenerator when the specific cooling power was increased. This change in the hot side temperature is a combination of several processes behind the tests. The first reason is that the sensitivity of the temperature-control cabinet is ± 0.5 K. Secondly, the fluid flow rate in the HEX was slightly too low to effectively remove the generated heat from the hot side during the cooling load tests. This began to be a concern only at tests with the specific cooling power above 10 W kg^{-1} when the utilisation factor was above 0.6. It means that the flow rate of the fluid in the HEX circuit was too

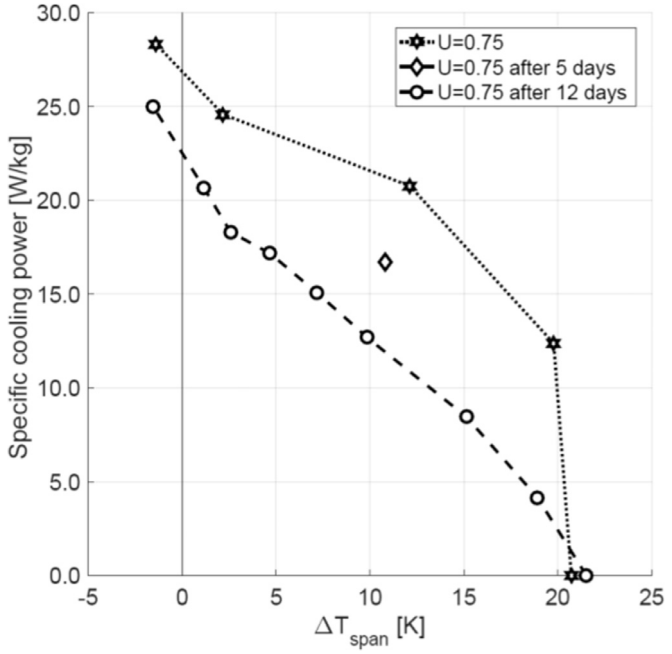

Fig. 10. Comparison of initial and repeated cooling power tests at $U = 0.75$ with five-layer regenerator at the constant hot side temperature of 303 K. The maximum applied cooling power for this regenerator was 3.5 W.

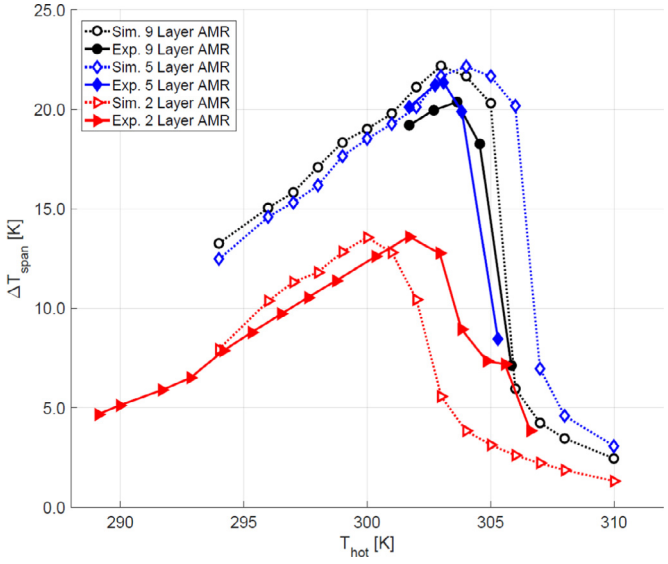

Fig. 11. The experimental steady state no-load temperature span between the hot and the cold side as a function of a constant hot side temperature and the modelling results.

low and could not remove the generated heat effectively at higher mass flow rates through the regenerator and higher applied cooling power.

Fig. 10 shows that the performance of the five-layer regenerator decreased after the initial test at utilisation of 0.75. In order to analyse the phenomenon, the cooling load test was repeated at $U = 0.75$ twice in the period of two weeks (Fig. 10). One can observe that the system performance at the latest test was the lowest. One month later, we found that the regenerator could not establish the initial temperature span at no-load tests and the system could not be drained. The blockage of the flow paths was possibly caused by mechanical breakdown of particles inside the bed. Thus, it was concluded that the regenerator disintegrated. The test on the nine-layer regenerator was also conducted in order to investigate its disintegration after three months. The regenerator could not reach steady state conditions and system could not be drained as well as the five-layer regenerator. However, a similar five-layer regenerator made of the $La(Fe,Si,Mn)_{13}H_y$ spherical particles, which was used for another study, showed no signs of mechanical degradation after a long term experiment (Lei et al., 2018). The regenerators were periodically tested for six months. Each time they were dried and stored at room temperature after a set of experiment was finished. One could note from Fig. 10 that the cooling power decreases while the temperature difference nearly does not change. This phenomenon could happen due to reduction of the utilisation during the cycle. The blockage of the flow paths caused maldistribution or reduction of the fluid mass flow, even though it was set to be the same.

We also investigated the possibility that regenerators lost their magnetocaloric properties after long-term experiments. VSM measurements were conducted for this purpose. No changes of magnetocaloric properties were found.

One also can observe that the decrease in performance is rather systematic. Figs. 8 and 10 show that five-layer regenerator performance after 12 days of testing at utilisation of 0.75 has similar trend as the initial performance at utilisation of 0.31. The mechanical breakdown of particles caused unfavourable changes in actual utilisation of the cycle.

It is evident from Fig. 1, that the five-layer regenerator lost a significant amount of mass from its top layer during the tests, as it was filled to the top of the housing before testing. This also happened to the nine-layer bed. Both regenerators were weighed after drying with pressurised air in the direction from the hot to cold side. The reason of this was to ensure that the regenerators were always dried in the same direction as well as secure that particles would not be removed from top layer by pressurised airflow. Note that all the regenerators were constructed from the cold side to the hot side allowing gravitational epoxy distribution. The five- and nine-layer regenerators lost 3.4% and 1.7% of their mass, respectively after testing. It is meaningful to emphasise that the temperature span in the regenerators are different for the beds with two layers and ones with five and nine layers. This is also linked to the increased magnetic forces due to increased mass of the used MCM and a larger T_C span over the beds. Thus, increasing the amount of epoxy in regenerators where the MCM must withstand larger magnetic forces should be considered.

Fig. 11 shows the modelling results compared with the experimental data set at no-load conditions. In general, good agreement is observed for all of the regenerators.

Even though the simulation results predicted an approximately 5 K broader working temperature range for both the five- and nine-layer regenerators, the overall prediction follows the trend and the maximum temperature span is well captured. From Fig. 11 it is evident that the model slightly under predicts the working temperature range for the regenerators with two layers. The maximum temperature span and the shape of the simulation curve fit the experimental data well, though. The slight shift in the performance curve might occur due to imperfections of the tested beds. It is widely discussed that the FOPT materials are very susceptible to variation in temperature range, Curie temperature distribution, or unevenness of the magnetocaloric properties in the MCM, etc. (Barcza et al., 2011; Lei et al., 2016, 2015; Lyubina et al., 2010). Numerical models are limited in predicting possible imperfections of a physical regenerator, such as uneven epoxy distribution, actual MCM particle size deviation, etc.

In this study, we showed that effectively using the layering technique, the FOPT materials could establish high performance under both no-load and cooling load conditions performance. Moreover, we presented the FOPT material, which established

the highest temperature span at no-load experiments and demonstrated the highest specific cooling power ever obtained using this small-scale testing device.

5. Conclusions

Six irregular particle $La(Fe,Mn,Si)_{13}H_y$ regenerators were tested in order to investigate the optimal amount of epoxy necessary to bond the MCM particles without compromising the performance and the effect of having multi-layered MCM regenerators. Firstly, four regenerators with two layers of MCM and a varying amount of epoxy were tested. It was concluded that 2 wt% gave the best trade-off between mechanical integrity and MCM/heat transfer performance. However, the regenerators with five and nine layers with 2 wt% of epoxy showed some mechanical degradation.

In this study, we show that layering the MCM does increase the performance of regenerators with FOPT materials. The two-layer regenerator showed a no-load temperature span of $\Delta T_{span} = 12.7$ K, while the five- and nine-layer regenerators showed no-load temperature spans of $\Delta T_{span} = 20.9$ K and $\Delta T_{span} = 20.7$ K, respectively. However, regenerators must be layered accurately and precisely in order to achieve the full benefits of the concept.

Experiments presented here show that $La(Fe,Mn,Si)_{13}H_y$ is a promising material for magnetic refrigeration. The material used in this study shows the highest temperature span of $\Delta T_{span} = 20.9$ K for no-load tests in comparison with other materials used in this small-scale device and also it exhibits the highest temperature span for a given cooling load $\Delta T_{span} = 19.8$ K at a heat load of 12.4 W kg^{-1}. This shows the significant potential for $La(Fe,Mn,Si)_{13}H_y$ to be used as regenerative material. However, the functional problems still exist when the material is used for long-term experiments. It is crucially important to overcome these problems in order to make $La(Fe,Mn,Si)_{13}H_y$ applicable in commercial devices.

Finally, the modelling results showed a good agreement with the experimental data with a slight offset in the range of working temperatures. The uncertainties between the experimental and modelling results are mainly due to inaccuracies in physical regenerators that the model cannot capture. However, generally good agreement between modelling and experimental data indicates that the regenerators generally functioned as expected and encourages using modelling as a beforehand tool to predict performance of materials.

Acknowledgements

This work was in part financed by the ENOVHEAT project, which is funded by Innovation Fund Denmark (Contract no. 12-132673).

References

Aprea, C., Cardillo, G., Greco, A., Maiorino, A., Masselli, C., 2015. A comparison between experimental and 2D numerical results of a packed-bed active magnetic regenerator. Appl. Thermal Eng. 90, 376–383. doi:10.1016/j.applthermaleng.2015.07.020.

Bahl, C.R.H., Navickaitė, K., Neves Bez, H., Lei, T., Engelbrecht, K., Bjørk, R., Li, K., Li, Z., Shen, J., Dai, W., Jia, J., Wu, Y., Long, Y., Hu, F., Shen, B., 2017. Operational test of bonded magnetocaloric plates. Int. J. Refrigeration 76, 245–251. doi:10.1016/j.ijrefrig.2017.02.016.

Bahl, C.R.H., Petersen, T.F., Pryds, N., Smith, A., 2008. A versatile magnetic refrigeration test device. Rev. Sci. Instrum. 79. doi:10.1063/1.2981692.

Barcza, A., Katter, M., Zellmann, V., Russek, S., Jacobs, S., Zimm, C., 2011. Stability and magnetocaloric properties of sintered $La(Fe,Mn,Si)_{13}H_z$ alloys. IEEE Trans. Magn. 47, 3391–3394. doi:10.1109/TMAG.2011.2147774.

Basso, V., Küpferling, M., Curcio, C., Bennati, C., Barzca, A., Katter, M., Bratko, M., Lovell, E., Turcaud, J., Cohen, L.F., 2015. Specific heat and entropy change at the first order phase transition of $La(FeMnSi)_{13}H$ compounds. J. Appl. Phys. 118, 53907. doi:10.1063/1.4928086.

Bez Neves, H., Navickaitė, K., Lei, T., Engelbrecht, K., Barcza, A., Bahl, R., H., C., 2016. Epoxy-bonded La(Fe,Mn,Si)13Hz as a multi layered active magnetic regenerator. doi:10.18462/iir.thermag.2016.0147

Bouchard, J., Nesreddine, H., Galanis, N., 2009. Model of a porous regenerator used for magnetic refrigeration at room temperature. Int. J. Heat Mass Transf. doi:10.1016/j.ijheatmasstransfer.2008.08.031.

Bratko, M., Lovell, E., Caplin, A.D., Basso, V., Barcza, A., Katter, M., Cohen, L.F., 2016. Determining the First Order Character of La(Fe,Mn,Si)13.

Brück, E., Tegus, O., Zhang, L., Li, X.W., De Boer, F.R., Buschow, K.H.J., 2004. Magnetic refrigeration near room temperature with Fe_2P-based compounds. J. Alloys Compd. 383, 32–36. doi:10.1016/j.jallcom.2004.04.042.

Engelbrecht, K., Nielsen, K.K., Bahl, C.R.H., Carroll, C.P., van Asten, D., 2013. Material properties and modeling characteristics for $MnFeP_{1-x}As_x$ materials for application in magnetic refrigeration. J. Appl. Phys. doi:10.1063/1.4803495.

Govindappa, P., Trevizoli, P.V, Campbell, O., Niknia, I., Christiaanse, T.V, Teyber, R., Misra, S., Schwind, M.A., van Asten, D., Zhang, L., Rowe, A., 2017. Experimental investigation of $MnFeP_{1-x}$ As_x multilayer active magnetic regenerators. J. Phys. D: Appl. Phys. 50, 315001. doi:10.1088/1361-6463/aa7a33.

Gschneidner, K.A., Pecharsky, V.K., 2008. Thirty years of near room temperature magnetic cooling: where we are today and future prospects. Int. J. Refrigeration 31, 945–961. doi:10.1016/j.ijrefrig.2008.01.004.

Jacobs, S., 2009. Modeling and optimal design of a multilayer active magnetic refrigeration system. In: Proceedings of 3rd International Conference on Magnetic Refrigeration at Room Temperature, pp. 267–273.

Jacobs, S., Russek, S., Auringer, J., Boeder, A., Chell, J., Komorowski, L., Leonard, J., Zimm, C., 2013. The Performance of Rotary Magnetic Refrigerators with Layered Beds of LaFeSiH 2, 21–27.

Jacobs, S., Auringer, J., Boeder, A., Chell, J., Komorowski, L., Leonard, J., Russek, S., Zimm, C., 2014. The performance of a large-scale rotary magnetic refrigerator. Int. J. Refrigeration 37, 84–91. doi:10.1016/j.ijrefrig.2013.09.025.

Kitanovski, A., Tušek, J., Tomc, U., Plaznik, U., Ožbolt, M., Poredoš, A., 2015. Magnetocaloric Energy Conversion. Springer, London doi:10.1007/978-3-319-08741-2.

Lanzarini, J., Barriere, T., Sahli, M., Gelin, J.C., Dubrez, A., Mayer, C., Pierronnet, M., Vikner, P., 2015. Thermoplastic filled with magnetocaloric powder. Mater. Des. 87, 1022–1029. doi:10.1016/j.matdes.2015.08.057.

Lei, T., Engelbrecht, K., Nielsen, K.K., Neves Bez, H., Bahl, C.R.H., 2016. Study of multilayer active magnetic regenerators using magnetocaloric materials with first and second order phase transition. J. Phys. D: Appl. Phys. 49, 345001. doi:10.1088/0022-3727/49/34/345001.

Lei, T., Engelbrecht, K., Nielsen, K.K., Veje, C.T., 2017. Study of geometries of active magnetic regenerators for room temperature magnetocaloric refrigeration. Appl. Thermal Eng. 111, 1232–1243. doi:10.1016/j.applthermaleng.2015.11.113.

Lei, T., Navickaite ˙, K., Engelbrecht, K., Barcza, A., Vieyra, H., Nielsen, K.., Bahl, C.. H., 2018. Passive Characterization and Active Testing of Epoxy Bonded Regenerators for Room Temperature Magnetic Refrigeration. doi:10.1016/j.applthermaleng.2017.08.152

Lei, T., Nielsen, K.K., Engelbrecht, K., Bahl, C.R.H., Neves Bez, H., Veje, C.T., 2015. Sensitivity study of multi-layer active magnetic regenerators using first order magnetocaloric material $La(Fe,Mn,Si)_{13}H_y$. J. Appl. Phys. 118, 0–8. doi:10.1063/1.4923356.

Liu, M., Yu, B., 2010. Numerical investigations on internal temperature distribution and refrigeration performance of reciprocating active magnetic regenerator of room temperature magnetic refrigeration ‘riques sur la distribution de la tempe´rature Etudes nume´ne´rateur. Int. J. Refrigeration 34, 617–627. doi:10.1016/j.ijrefrig.2010.12.003.

Lyubina, J., Schäfer, R., Martin, N., Schultz, L., Gutfleisch, O., 2010. Novel design of $La(Fe,Si)_{13}$ alloys towards high magnetic refrigeration performance. Adv. Mater. 22, 3735–3739. doi:10.1002/adma.201000177.

Monfared, B., Palm, B., 2015. Optimization of layered regenerator of a magnetic refrigeration device. Int. J. Refrigeration 57, 103–111. doi:10.1016/j.ijrefrig.2015.04.019.

Mugica Guerrero, I., Poncet, S., Bouchard, J., Mugica Guerrero, I., Poncet, S., Bouchard, J., 2017. Entropy generation in a parallel-plate active magnetic regenerator with insulator layers. J. Appl. Phys. 74901. doi:10.1063/1.4975818.

Nielsen, K.K., Engelbrecht, K., 2012. The influence of the solid thermal conductivity on active magnetic regenerators. J. Phys. D: Appl. Phys. doi:10.1088/0022-3727/45/14/145001.

Plaznik, U., Tušek, J., Kitanovski, A., Poredoš, A., Tu, J., Kitanovski, A., Poredo, A., 2013. Numerical and experimental analyses of different magnetic thermodynamic cycles with an active magnetic regenerator. Appl. Thermal Eng. 59, 52–59. doi:10.1016/j.applthermaleng.2013.05.019.

Richard, M.A., Rowe, A.M., Chahine, R., 2004. Magnetic refrigeration: Single and multimaterial active magnetic regenerator experiments. J. Appl. Phys. 95, 2146–2150. doi:10.1063/1.1643200.

Smith, A., Bahl, C.R.H., Bjork, R., Engelbrecht, K., Nielsen, K.K., Pryds, N., 2012. Materials challenges for high performance magnetocaloric refrigeration devices. Adv. Energy Mater. 2, 1288–1318. doi:10.1002/aenm.201200167.

Teyber, R., Trevizoli, P.V., Christiaanse, T.V., Govindappa, P., Niknia, I., Rowe, A., 2016. Performance evaluation of two-layer active magnetic regenerators with second-order magnetocaloric materials. Appl. Thermal Eng. 106, 405–414. doi:10.1016/j.applthermaleng.2016.06.029.

Trevizoli, P.V, Nakashima, A.T., Barbosa Jr., J.R., 2016. Performance evaluation of an active magnetic regenerator for cooling applications – part II: mathematical modeling and thermal losses Évaluation de la performance d ’ un régénérateur magnétique actif pour les applications de refroidissement – Partie II. Int. J. Refrigeration 72, 206–217. doi:10.1016/j.ijrefrig.2016.07.010.

Tura, A., Nielsen, K.K., Rowe, A., 2012. Experimental and modeling results of a parallel plate-based active magnetic regenerator. Int. J. Refrigeration. doi:10.1016/j.ijrefrig.2012.04.016.

Tušek, J., Kitanovski, A., Tomc, U., Favero, C., Poredoš, A., 2014. Experimental comparison of multi-layered La–Fe–Co–Si and single-layered Gd active magnetic regenerators for use in a room-temperature magnetic refrigerator. Int. J. Refrigeration 37, 117–126. doi:10.1016/j.ijrefrig.2013.09.003.

Vuarnoz, D., Kawanami, T., 2013. Experimental validation of a coupled magneto-thermal model for a fl at-parallel-plate active magnetic regenerator. Appl. Thermal Eng. 54, 433–439. doi:10.1016/j.applthermaleng.2013.01.007.

Zimm, C., Boeder, A., Chell, J., Sternberg, A., Fujita, A., Fujieda, S., Fukamichi, K., 2005. Design and performance of a permanent magnet rotary refrigerator. In: Proceedings of the 1st International Conference on Magnetic Refrigeration at Room Temperature, pp. 367–373.